Explainable Fuzzy Learning for Cardiac Segmentation in 3D Short-Axis MRI

Anh-Cang Phan[1], Van-Hung Nguyen[2], Thi-My-Nga Nguyen[1]
[1] Vinh Long University of Technology Education, Vinh Long, Vietnam
[2] Dong Thap Medical College, Dong Thap, Vietnam
Correspondence: Anh-Cang Phan, cangpa@vlute.edu.vn
Communication: received 30 June 2025, revised 28 August 2025, accepted 01 October 2025
Digital Object Identifier: https://doi.org/10.32913/mic-ict-research.v2025.n3.1401

Abstract: Accurate segmentation in short-axis cardiac MRI is crucial for extracting parameters to diagnose cardiovascular diseases. However, deep learning models often use Max or Average pooling to reduce feature map size, risking loss of important information. In addition, most current research focuses mainly on the segmentation accuracy of machine learning models, while lacking interpretation of the segmentation results - a critical factor for clinical applications. In this study, we propose a fuzzy deep learning model called 3DMFL-Net, which combines Explainable AI (XAI) techniques to segment cardiac structures including the Left Ventricle, Myocardium, and Right Ventricle from 3D short-axis MRI images, while also providing interpretation of the segmentation results. The model adopts a 3D fuzzy pooling method to replace traditional pooling methods. The 3D fuzzy pooling leverages fuzzy logic along with a Gaussian membership function to identify important features within the pooling window, allowing reduction of the feature map size while preserving essential information. To visualize and interpret the model's decisions, we apply XAI with the 3D Grad-CAM method to generate heatmaps that highlight the important image regions involved in the segmentation process of the proposed model. The proposed model is evaluated on the M&Ms-2020 dataset, which includes multiple 3D cardiac MRI scans across various disease groups and is provided by different device vendors. The results show that the Dice coefficient reaches 84.6% for the left ventricle, 76.6% for the myocardium, and 79.5% for the right ventricle. The proposed method suits intelligent healthcare deployment and helps clinicians trust segmentation outcomes.

Keywords: *Fuzzy deep learning, Explainable AI (XAI), 3D fuzzy pooling*

I. Introduction

1. Practical Basis

According to WHO [1], cardiovascular diseases cause around 17.9 million deaths annually, making them the leading global cause of death. Accurate segmentation of LV, MYO, and RV in 3D cardiac MRI is crucial for heart disease classification but is labor-intensive manually. Deep learning has improved analysis by extracting features and reducing dimensions via conventional pooling. This approach may lead to the loss of important information [2], whereas fuzzy pooling has shown strong capability in handling uncertainty in medical data within pooling regions [3]. Moreover, most current studies focus only on MRI segmentation accuracy without providing interpretability of the results based on image features - a critical factor in clinical applications [11]. To address these issues, we propose a fuzzy deep learning model called 3DMFL-Net (3D Max Fuzzy Light U-Net) to segment cardiac structures such as LV, MYO, and RV from 3D short-axis cardiac MRI at two cardiac phases: End-Diastolic (ED) and End-Systolic (ES). The model incorporates the proposed 3D fuzzy pooling technique to accurately identify important features within pooling windows, enabling dimensionality reduction while preserving essential information. To interpret segmentation results, we use 3D Grad-CAM with XAI to generate heatmaps highlighting regions influencing 3DMFL-Net's decisions.

2. Related Works

To better exploit the inter-slice spatial information in 3D cardiac MRI data and improve segmentation accuracy, Liu Tao et al. [15] proposed the Bi-CLSTM (Bidirectional Convolutional Long Short-Term Memory) neural network model, which segments each slice of short-axis cardiac 3D MRI images. The Bi-CLSTM model leverages convolutional neural networks to compress intra-slice information, while the bidirectional convolutional LSTM captures inter-slice relationships across two time points: end-diastole (ED) and end-systole (ES). From the resulting 3D segmentations, Liu Tao et al. extracted key physiological cardiac indices, including left ventricular ejection fraction (LVEF), left ventricular volume at ED, right ventricular

ejection fraction (RVEF), right ventricular volume at ED and ES, total myocardial mass at ED and ES, and the ratio of total ventricular volume to myocardial mass at ED. These indices were then used to classify several cardiac conditions including DCM, HCM, MINF, RV, and NOR using the proposed algorithm. Experiments on the ACDC 2017 dataset showed that the Bi-CLSTM model achieved Dice coefficients of 91.0% (LV), 86.5% (MYO), and 89.0% (RV), with a classification accuracy of 94% on the test set.

Jelmer M. Wolterink et al. [14] introduced a basic convolutional neural network (CNN) to segment individual slices from short-axis cardiac MRI images at ED and ES with achieved Dice coefficients of 94% (LV), 87.0% (MYO), and 88.0% (RV), and a classification accuracy of 91% on the test dataset. Fabian Isensee et al. [16] proposed a deep learning network inspired by both 2D and 3D UNet architectures for segmenting LV, MYO, and RV structures. Their experiments on the ACDC 2017 dataset involved a 3D input of size 10x244x244 voxels (depth, width, height), trained for 300 epochs using five-fold cross-validation with the Adam optimizer and cross-entropy loss with achieved Dice scores of 95.0% (LV), 91.1% (MYO), and 92.3% (RV), with a classification accuracy of 92%. Yakun Chang et al. [13] proposed a method to classify cardiac conditions (DCM, HCM, MINF, RV, NOR). Initially, LV, MYO, and RV regions were detected using a YOLO network at both ED and ES phases. These regions were then segmented using a fully convolutional network (FCN) into four classes: LV, MYO, RV, and background. Seven key indices were extracted from the segmentations, including ventricular volumes at ED and ES, ejection fractions, LV/RV volume ratios, and myocardial volumes, along with height and weight. These features were fed into a fully connected neural network for classification. The method achieved Dice scores of 91.9% (LV), 87.8% (MYO), and 86.9% (RV), with a classification accuracy of 90%. Adi Wibowo et al. [17] proposed an EfficientNetB5-UNet architecture to segment short-axis cardiac MRI slices from the ACDC 2017 dataset. A custom two-dimensional thickness algorithm was developed to fuse segmentations into 2D representations of the heart at ED and ES. These were used for few-shot learning classification of DCM, HCM, MINF, RV, and NOR. The model achieved Dice scores of 93.0% (LV), 89.8% (MYO), and 89.9% (RV), with a classification accuracy of 90%. Xiao Liu et al. [19] proposed the SDNet model combined with a resolution-based data augmentation strategy to enhance generalization for cardiac MRI segmentation. SDNet was evaluated on the M&Ms dataset, achieving Dice scores of 88.1% for the left ventricle (LV), 83.1% for the myocardium (MYO), and 80.0% for the right ventricle (RV). In addition, Cian M. Scannell et al. [20] introduced an improved variant of the 2D U-Net model, trained using a domain-adversarial learning approach that leverages both labeled and unlabeled data for cardiac structure segmentation in MRI images. Results on the M&Ms dataset showed that the model achieved Dice scores of 88% for LV, 80% for MYO, and 84% for RV.

II. Background

1. Anatomical Structures in Short-Axis Cardiac MRI

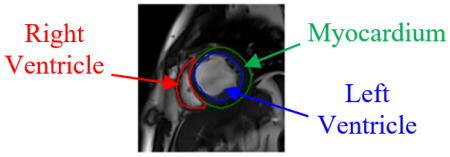

Figure 1: LV, MYO, RV structures on MRI (slice 5, ED phase)

Short-axis cardiac MRI images include three key regions: LV, MYO, and RV [7]. Fig. 1 shows these structures at slice 5 during the ED phase for patient S1S3Z7 from the M&Ms-2020 dataset. The cardiac cycle has two phases: systole, when ventricles contract, and diastole, when they relax and fill with blood [8]. ES represents minimum ventricular volume, and ED the maximum. Fig. 2 illustrates LV, MYO, and RV at slice 4 during ED and ES phases for patient M4P7Q6 from the same dataset [7].

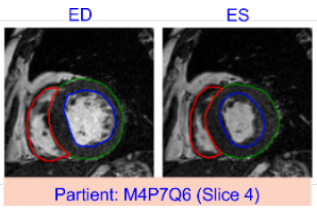

Figure 2: LV, MYO, RV structures on MRI

2. Model Evaluation Metrics

The Dice coefficient (Dice) is used to evaluate the similarity between the segmented region and the ground truth in the image, and is calculated using Equation (1). The Cross-Entropy loss function (LCE) is used to optimize the model by minimizing the difference between predicted values and ground truth, as described in Equation (2).

$$Dice = \frac{2 \times |A \cap B|}{|A| + |B|} \tag{1}$$

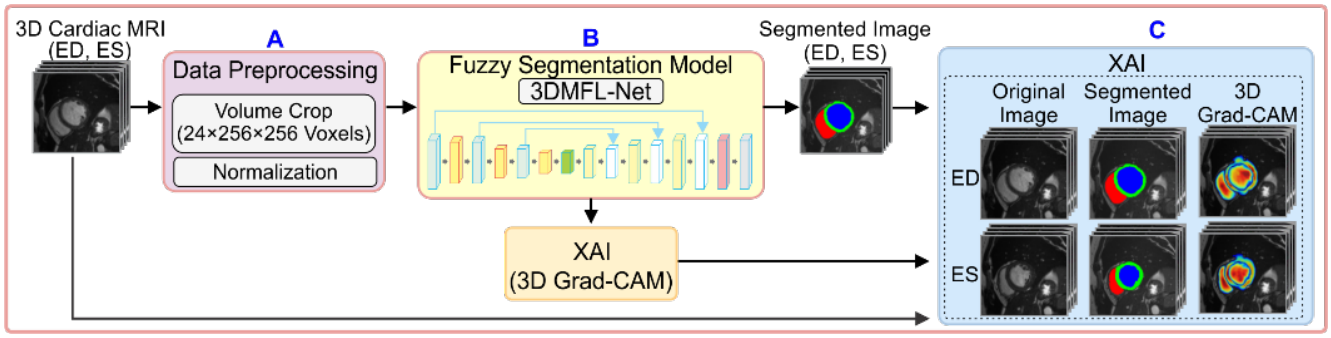

Figure 3: The overall proposed method for segmenting short-axis 3D cardiac MRI

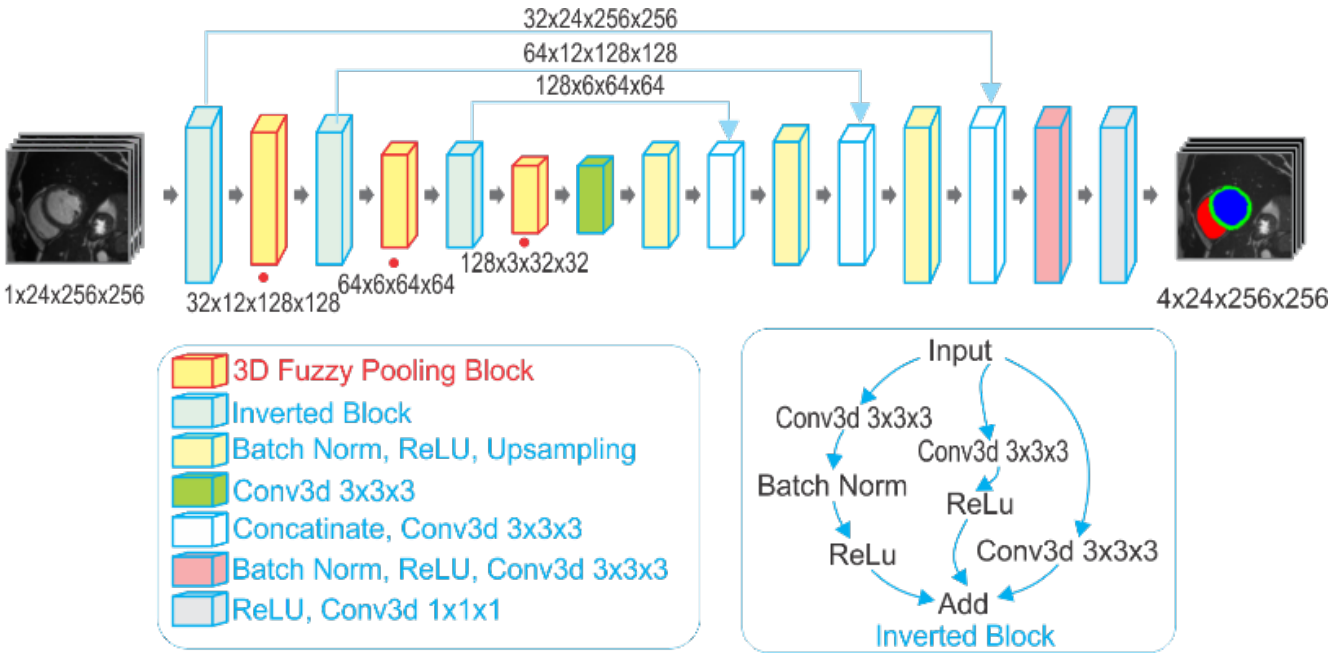

Figure 4: The proposed fuzzy deep learning network model 3DMFL-Net

$$LCE = -\frac{1}{N}\sum_{i=1}^{N}\sum_{c=1}^{C} y_{i,c}\log(p_{i,c}) \tag{2}$$

Where A is the set of predicted voxels, B is the set of ground truth voxels, N is the total number of image pixels, $p_{i,c} \in [0,1]$ is the predicted probability that pixel i belongs to class c, and $y_{i,c} \in \{0,1\}$ is the ground truth label of pixel i.

III. Proposed Method

1. Pre-processing

In part A of Fig. 3, MRI images from various scanners are standardized to a region of interest (ROI) of size 24x256x256 through zero-padding or central cropping. Voxel intensities are then normalized to a range between 0 and 1.

2. Proposed 3D Max Fuzzy Light U-Net (3DMFL-Net) Network Model

In part B of Fig. 3, we propose 3DMFL-Net, a fuzzy deep learning model improved from Light U-Net by Mehreen Irshad et al. in 2023 [9], designed for the segmentation of LV, MYO, and RV in short-axis 3D cardiac MRI. 3DMFL-Net consists of two main components, the encoder and the decoder, as detailed in Fig. 4.

In the encoder, the number of feature maps increases from 1 to 256, while the spatial resolution is progressively reduced from 24x256x256 to 3x32x32 voxels [12]. The encoder includes three Inverted blocks and a final convolutional layer with a 3x3x3 voxel kernel. Each Inverted block contains three parallel convolutional branches: the first uses a 3x3x3 kernel with batch normalization and ReLU activation; the second applies a 3x3x3 convolution followed by ReLU; and the third performs a single 3x3x3 convolution.

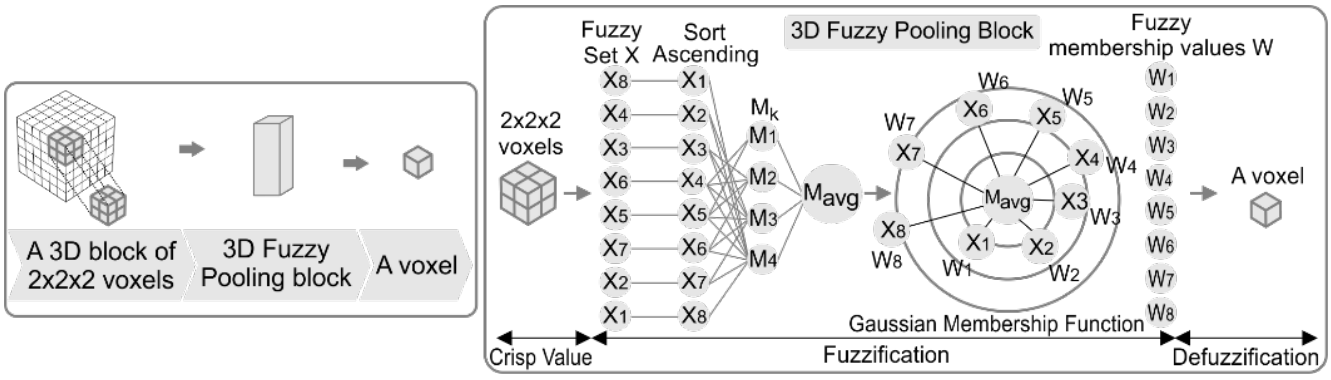

Figure 5: The proposed 3D fuzzy pooling method

The outputs of these three branches are summed to form the final output of each block. After the three Inverted blocks, a 3D fuzzy pooling layer is applied instead of max pooling to downsample the feature maps while preserving essential information. The fuzzy pooling process is illustrated in Fig. 5.

A deep convolutional layer is then added at the end of the encoder to enhance feature representation. The decoder uses convolutional layers and stride-2 upsampling to restore spatial resolution and reduce feature maps. Specifically, the 3D fuzzy pooling method employs fuzzy set theory from fuzzy logic to determine the degree of membership of features within the pooling window. It uses the Gaussian Membership Function (GMF), defined in Equation (6), to assign a membership value ranging from 0 to 1 for each element, where a value closer to 1 indicates a stronger membership in the fuzzy set, and vice versa. 3D fuzzy pooling involves three main stages: crisp value identification, fuzzification, and defuzzification. In the first stage, crisp value identification, a 3D pooling block of size 2x2x2 voxels is selected from the feature map, and eight voxel values are extracted. In the second stage, fuzzification, each of the eight extracted values is assigned a symbol from x_1 to x_8. Let $X = \{x_1, x_2, x_3, x_4, x_5, x_6, x_7, x_8\}$ be the set of values extracted in Stage 1, which is treated as a fuzzy set. The values in X are sorted in ascending order to highlight the overall data trend and reduce noise influence. The overall mean value (m_{avg}) of the fuzzy set X is then computed using Equation (4), which averages the local means m_k defined in Equation (3). Next, the Gaussian Membership Function is applied to calculate the membership values for each element in X, resulting in the membership set $W = \{w_1, w_2, w_3, w_4, w_5, w_6, w_7, w_8\}$, representing the degree of belonging of each corresponding element in X. The third stage, defuzzification, uses sets X and W to estimate the output of the pooling operation, denoted as P_{pooling}. This value represents the membership of fuzzy set X, as shown in Equation (7).

$$m_k(X) = \frac{1}{2k} \sum_{i=q-k+1}^{q+k} x_i \tag{3}$$

$$m_{\text{avg}} = \frac{1}{q} \sum_{k=1}^{q} m_k \tag{4}$$

$$\sigma_X = \sum_{i=1}^{n} |x_i - m_{\text{avg}}| \tag{5}$$

$$w_i = \mathbf{e}^{-\frac{(x_i - m_{\text{avg}})^2}{2\sigma_X^2}} \tag{6}$$

$$P_{\text{pooling}} = \max(w_i x_i) \tag{7}$$

Here, n represents the number of elements in the fuzzy set X; $q = n/2$ is a constant used to determine the subset size of X for computing the local means m_k. The variable k denotes the number of local means computed, with the condition $1 \leq k \leq q$. The symbol x_i denotes the value of the i-th element in the fuzzy set X. The corresponding membership degree of the i-th element in X is represented by w_i, where i indicates the position of the element within the set. σ_X refers to the variance of the fuzzy set X, which measures the dispersion of the features around the overall mean value m_{avg}.

3. Interpretation of the Segmentation Results

In part C of Fig. 3, the interpretation process includes: (a) visualizing 3D short-axis cardiac MRI images at two key physiological phases, ED and ES; (b) displaying segmentation results with clearly color-coded regions to support visual interpretation, including LV in blue, MYO in green, and RV in red; and (c) generating heatmaps using the 3D Grad-CAM method as described in [10]. The heatmaps are color-coded from blue to red, where red indicates

regions with high influence on the model's decision and blue indicates less attention.

IV. Experiments and Evaluation of the Proposed Method

1. Installation Environment, Dataset, and Model Training Parameters

The experiments were conducted on Google Colab using an A100 GPU with 40 GB of GPU RAM. The M&Ms-2020 dataset [7] consists of 345 patients, each with two 3D short-axis cardiac MRI scans corresponding to the ED and ES phases. The dataset includes images acquired from MRI scanners produced by four different vendors, labeled as Vendor A, Vendor B, Vendor C, and Vendor D. The dataset includes images acquired from MRI scanners produced by four different vendors, labeled as Vendor A, Vendor B, Vendor C, and Vendor D. The 3DMFL-Net segmen-tation model was trained for 200 epochs with a learning rate of 1e-4. It was set to classify three classes: LV, MYO, and RV, and used a batch size of 2 during training (See Table I).

TABLE I: The number of short-axis 3D cardiac MRI images in the M&Ms-2020 experimental dataset.

	Vendor A		Vendor B		Vendor C		Vendor D		Total
	ED	ES	ED	ES	ED	ES	ED	ES	
Training	75	75	75	75	25	25	0	0	350
Validation	4	4	10	10	10	10	10	10	68
Testing	16	16	40	40	40	40	40	40	272
Total	95	95	125	125	75	75	50	50	690

2. Training Results

Fig. 6 presents training loss and Dice trends. (a) The model reduced loss to 0.004 on training and 0.026 on validation at epoch 195. (b) It achieved 90.4% Dice on training and 74.9% on validation at the same epoch. Total training time was 296 minutes.

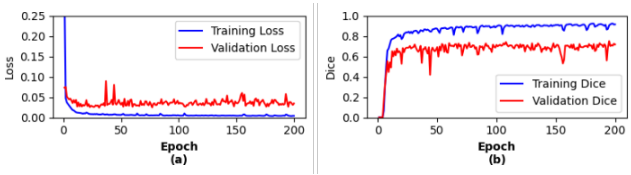

Figure 6: Chart of Loss values and Dice coefficients during model training

3. Testing Results

TABLE II: Dice coefficient (%) on the testing set by different device vendors.

Model	Vendor	LV	MYO	RV	Mean
3DMFL-Net	A	81.8	68.8	70.8	73.8
	B	84.6	76.6	79.5	80.2
	C	75.3	65.6	63.8	68.2
	D	69.5	56.2	60.8	62.2

Table II presents the Dice coefficients for the LV, MYO, and RV regions, showing that 3DMFL-Net achieved an average of 71.1%. Notably, on MRI data from Vendor B, the model achieved 84.6% for LV, 76.6% for MYO, and 79.5% for RV, demonstrating strong performance across various data sources. Table III compares pooling methods using the same 3DMFL-Net model. The fuzzy pooling method achieved the highest average Dice score of 71.1%, followed by max pooling with 70.2% and average pooling with 69.3%, indicating the advantage of fuzzy pooling in preserving spatial information during feature map down-sampling. These results are statistically robust, with the observed performance within the 96% confidence interval, indicating that the outcomes are stable and unlikely to be due to random variation.

Although 3DMFL-Net demonstrates strong performance across most vendors, the model exhibits lower Dice scores on data from Vendor D. It should be noted that these data were not included in the training set and were only used in the test set, according to the design of the M&Ms-2020 dataset to evaluate model generalization. Consequently, the reduced performance is expected and reflects the challenges of applying the model to unseen data with different imaging characteristics.

TABLE III: Dice coefficient (%) on the testing set by different pooling methods.

Proposed Model	Pooling method	LV	MYO	RV	Mean
3DMFL-Net	Average pooling	76.9	64.0	67.0	69.3
	Max pooling	78.0	66.4	66.2	70.2
	3D Fuzzy pooling	77.8	66.8	68.7	71.1

Fig. 7 shows 3DMFL-Net results on patient I5L3S2 from Vendor B at the ED and ES phases. The longitudinal view includes 9 slices at ED and 8 at ES; slices 1, 5, and 9 in ED, and slices 1, 5, and 8 in ES highlight heart morphology changes. We present the interpretability process of the 3DMFL-Net model for patient I5L3S2 from the M&Ms-2020 testing set, as illustrated in Fig. 8.

In addition to displaying slices on the original images, the segmentation results at two key physiological

TABLE IV: Segmentation performance comparison between the proposed model and related work.

Authors	Methods	LV	MYO	RV	Mean	XAI	Parameters
Lei Li et al. [4]	STDGNs	76.6	71.5	63.6	70.5	–	–
Italo Francyles Santos da Silva et al. [5]	EAIS-Net, IRAX-Net	83.3	74.6	70.8	76.2	–	–
Jiapeng Li et al. [6]	UDA	79.0	88.1	86.3	84.4	–	–
Xiao Liu et al. [19]	FS SDNet + RA	88.1	83.1	80.0	83.7	–	–
Cian M. Scannell et al. [20]	2D U-Net	88.0	80.0	84.0	84.0	–	–

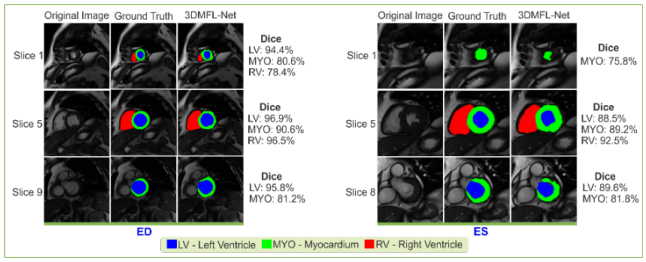

Figure 7: Slice-by-slice segmentation results of patient I5L3S2 at the ED and ES phases

phases, ED and ES, are also shown. Three main anatomical structures are highlighted: the LV in blue, the MYO in green, and the RV in red, demonstrating a high degree of correspondence with the original anatomical features. Furthermore, the heatmaps generated using the 3D Grad-CAM method reveal that the most influential regions in the segmentation process, highlighted in dark red, are primarily concentrated in the LV, MYO, and RV. The color gradually shifts to blue, indicating a lower level of influence, with blue areas representing regions less attended to by the model. Displaying heatmaps on individual 3D MRI slices enables clinicians to track the model's attention through image depth. ED and ES phases are shown separately for direct visual comparison across the cardiac cycle. This supports accurate interpretation and verification, playing an important role in developing a reliable intelligent AI system for clinical applications.

4. Comparison and Discussion

Table IV shows that the 3DMFL-Net model achieved an average Dice coefficient of 71.1% across the LV, MYO, and RV regions, which is higher than the 70.5% reported by Lei Li et al. [4]. A key advantage of the proposed method is its interpretability, enabling direct visualization and verification of segmentation results on medical images. In contrast, most existing methods lack explainability, potentially limiting their reliability in clinical use. With only 3.49 million parameters, 3DMFL-Net features a lightweight and optimized architecture, enhancing processing speed and enabling easy integration into smart healthcare systems.

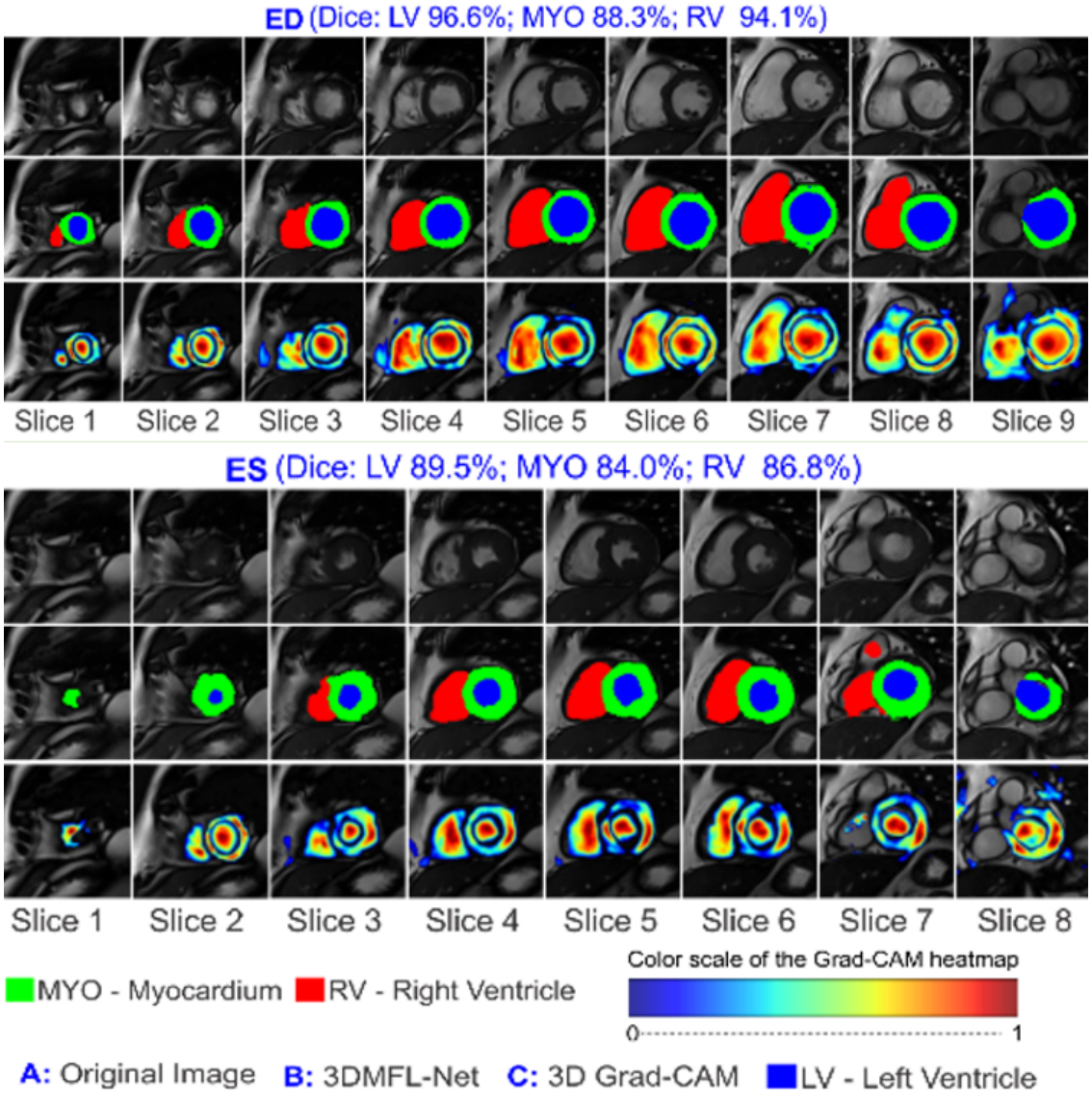

Figure 8: Explaining the segmentation results of patient I5L3S2 at both ED and ES phases

V. Conclusion

In this study, we propose a lightweight fuzzy deep learning model, 3DMFL-Net, which integrates explainable AI to segment the LV, MYO, and RV, thereby enhancing the interpretability of the segmentation results. The main contributions of this study are as follows: (a) A 3D fuzzy pooling method is proposed using a Gaussian membership function to reduce the size of feature maps while preserving critical features, demonstrating advantages over max pooling and average pooling in deep learning models; (b) Developing the Light U-Net model from 2D to 3D while integrating the 3D fuzzy pooling method to enhance segmentation performance in three-dimensional space; (c) The proposed fuzzy segmentation model, 3DMFL-Net, incorporates XAI to assist clinicians in segmenting cardiac structures and to provide image-based interpretability. Experimental results on the M&Ms-2020 dataset show that the proposed method achieves Dice coefficients of 84.6% for LV, 76.6% for MYO, and 79.5% for RV on 3D cardiac MRI images from Vendor B. These results show the proposed model effectively segments diverse medical data, including noisy inputs, and its lightweight design suits deployment in smart healthcare systems.

References

[1] World Health Organization, https://www.who.int/health-topics/cardiovascular-diseases, last accessed 2025/06/10.

[2] Chen, C., Qin, C., Qiu, H., Tarroni, G., Duan, J., Bai, W., & Rueckert, D. Deep learning for cardiac image segmentation: a review. *Frontiers in Cardiovascular Medicine*, 7, 25, 2020.

[3] Yuniarno, E. M., Purnama, I. K. E., Aritsugi, M., & Purnomo, M. H. Investigating diverse loss functions for myocardium ring segmentation in Cardiac Magnetic Resonance images using fuzzy pooling. *Array*, 26, 100382, 2025.

[4] Li, L., Zimmer, V. A., Ding, W., Wu, F., Huang, L., Schnabel, J. A., & Zhuang, X. Random style transfer based domain generalization networks integrating shape and spatial information. In *Statistical Atlases and Computational Models of the Heart. M&Ms and EMIDEC Challenges: 11th International Workshop, STACOM 2020, Held in Conjunction with MICCAI 2020, Lima, Peru, October 4, 2020, Revised Selected Papers 11* (pp. 208-218). Springer International Publishing, 2021.

[5] Silva, I. F. S. D., Silva, A. C., Paiva, A. C. D., Gattass, M., & Cunha, A. M. A Multi-Stage Automatic Method Based on a Combination of Fully Convolutional Networks for Cardiac Segmentation in Short-Axis MRI. *Applied Sciences*, 14(16), 2024.

[6] Li, J., Lv, Y., Xu, L., & Qi, L. An Unsupervised Domain Adaptation Model Based on Multi-Level Joint Alignment for Multi-Modal Cardiac Image Segmentation. *Procedia Computer Science*, 226, 106-112, 2023.

[7] Campello, V. M., Gkontra, P., Izquierdo, C., Martin-Isla, C., Sojoudi, A., Full, P. M., & Lekadir, K. Multi-centre, multi-vendor and multi-disease cardiac segmentation: the M&Ms challenge. *IEEE Transactions on Medical Imaging*, 40(12), 3543-3554, 2021.

[8] Flores-Alonso, S. I., Tovar-Corona, B., & Luna-García, R. Deep learning algorithm for heart valve diseases assisted diagnosis. *Applied Sciences*, 12(8), 3780, 2022.

[9] Irshad, M., Yasmin, M., Sharif, M. I., Rashid, M., Sharif, M. I., & Kadry, S. A novel light u-net model for left ventricle segmentation using MRI. *Mathematics*, 11(14), 3245, 2023.

[10] Gunashekar, D. D., Bielak, L., Hägele, L., Oerther, B., Benndorf, M., Grosu, A. L., & Bock, M. Explainable AI for CNN-based prostate tumor segmentation in multi-parametric MRI correlated to whole mount histopathology. *Radiation Oncology*, 17(1), 65, 2022.

[11] Wolterink, J. M., Leiner, T., Viergever, M. A., & Isgum, I. Automatic Segmentation and Disease. 4, 12, 2024.

[12] Rao, V. M., Wan, Z., Arabshahi, S., Ma, D. J., Lee, P.-Y., Tian, Y., Zhang, X., Laine, A. F., & Guo, J. Improving Across-Dataset Brain Tissue Segmentation Using Transformer. 31, 1, 2023.

[13] Chang, Y., Song, B., Jung, C., & Huang, L. Automatic segmentation and cardiopathy classification in cardiac MRI images based on deep neural networks. *2018 IEEE International Conference on Acoustics, Speech and Signal Processing (ICASSP)*, 15 Apr. 2018.

[14] Wolterink, J. M., Leiner, T., Viergever, M. A., & Isgum, I. Automatic Segmentation and Disease. 3 Aug. 2020.

[15] Tao, L., Tian, Y., Zhao, S., Huang, X., & Qingjun, W. Residual Convolutional Neural Network for Cardiac Image Segmentation and Heart Disease Diagnosis. *IEEE Access*, 8, 2020.

[16] Isensee, F., Jaeger, P. F., Full, P. M., Wolf, I., Engelhardt, S., & Maier-Hein, K. H. Automatic Cardiac Disease Assessment on cine-MRI via Time-Series Segmentation and Domain Specific Features. 25 Jan. 2018.

[17] Wibowo, A., Triadyaksa, P., Sugiharto, A., Sarwoko, E. A., Nugroho, F. A., Arai, H., & Kawakubo, M. Cardiac Disease Classification Using Two-Dimensional. *Journal of Imaging*, 194, 2022.

[18] Cepova, L., Elangovan, M., Ramesh, J. N., Chohan, M. K., Verma, A., & Mohammad, F. Improving privacy preserving multi-faceted long short term memory for accurate evaluation of encrypted time series MRI images in heart disease. *Scientific Reports*, 14, 30 Aug. 2024.

[19] Liu, X., Thermos, S., Chartsias, A., O'Neil, A., & Tsaftaris, S. A. Disentangled representations for domain-generalized cardiac segmentation. In *International Workshop on Statistical Atlases and Computational Models of the Heart* (pp. 187-195). Cham: Springer International Publishing, 2020.

[20] Scannell, C. M., Chiribiri, A., & Veta, M. Domain-adversarial learning for multi-centre, multi-vendor, and multi-disease cardiac MR image segmentation. In *International Workshop on Statistical Atlases and Computational Models of the Heart* (pp. 228-237). Cham: Springer International Publishing, 2020.

Assoc. Prof. Dr. Anh-Cang Phan is a lecturer at Vinh Long University of Technology Education, Vietnam. He received his Ph.D. in Informatics from Aix-Marseille University, France, and was conferred the title of Associate Professor in 2023. His research interests cover a wide range of topics, including Machine Learning, Deep Learning, Big Data, and 3D Modeling, with a strong focus on developing intelligent systems that bridge the gap between theory and real-world applications. Over the years, Dr. Phan has conducted numerous practical and interdisciplinary research projects, particularly in smart agriculture, intelligent irrigation systems, and medical image processing applications that have been successfully implemented in several hospitals across Vietnam. His works contribute significantly to advancing digital transformation in both the agricultural and healthcare sectors. He is also the author of the useful solution "Automatic Irrigation Control System," which was patented by the Intellectual Property Office of Vietnam for its innovative approach to enhancing agricultural efficiency through automation and intelligent control. In 2020, Dr. Phan was listed in the Vietnam Yellow Book of Innovation by the Ministry of Science and Technology, recognizing his outstanding contributions to scientific research, innovation, and technological development in Vietnam.
Email: cangpa@vlute.edu.vn

Nguyen Thi-My-Nga received a Bachelor's degree in Software Engineering from Can Tho University in 2013 and a Master's degree in Computer Science from Can Tho University, Vietnam, in 2019. She is currently a Lecturer at the Faculty of Information Technology, Vinh Long University of Technology and Education, Vietnam. Her research interests include Machine Learning, Deep Learning, and Medical Diagnostic Systems.
Email: ngantm@vlute.edu.vn

Van-Hung Nguyen is a student in the Master of Information Technology program at the Faculty of Information Technology, Vinh Long University of Technology Education. He is currently working at Dong Thap Medical College. His research interests include Machine Learning, Deep Learning, and Computer Vision.
Email: nvhung8698@gmail.com